Science of the Total Environment 912 (2024) 169620

Contents lists available at ScienceDirect

Science of the Total Environment

journal homepage: www.elsevier.com/locate/scitotenv

Detecting soil water redistribution in subsurface drip irrigated processing tomatoes using electrical resistivity tomography, proximal sensing and hydrological modelling

Iael Raij-Hoffman [a,b], Daniela Vanella [c,*], Juan Miguel Ramírez-Cuesta [c,d], Srinivasa Rao Peddinti [a,b], Isaya Kisekka [a,b]

[a] Department of Land Air & Water Resources, University of California Davis, Davis, CA 95616, USA
[b] Department of Biological and Agricultural Engineering, University of California Davis, Davis, CA 95616, USA
[c] Dipartimento di Agricoltura, Alimentazione e Ambiente (Di3A), Università degli Studi di Catania, Via S. Sofia, 100, Catania 95123, Italy
[d] Departamento de Ecología, Centro de Investigaciones sobre Desertificación (CIDE, CSIC-UV-GV), Moncada, Spain

HIGHLIGHTS

- Soil water redistribution was determined under field conditions by multiple methods.
- Time-lapse ERT surveys were performed at two transects during an irrigation event.
- Integrating proximal sensing data enhanced crop water status identification.
- Hydrus 2D and ERT both showed simultaneous wetting and root water uptake processes.

GRAPHICAL ABSTRACT

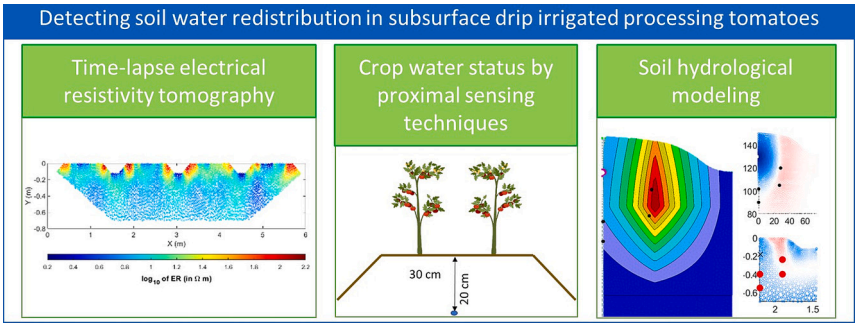

ARTICLE INFO

Editor: Charlotte Poschenrieder

Keywords:
Soil-plant-atmosphere continuum
Soil moisture
ERT tomography
Soil hydrological modelling
Subsurface drip irrigation

ABSTRACT

In this study, multiple soil-plant-atmosphere *continuum* (SPAC) monitoring methodologies, including electrical resistivity tomography (ERT), proximal thermal sensing techniques, and micrometeorological data, were combined with two-dimensional (2-D) soil hydrological modelling using HYDRUS 2-D to explore the soil water redistribution, and infer the relative crop water status in a subsurface drip irrigated (SDI) processing tomato field located in California (Yolo County, USA). Specifically, time-lapse ERT surveys were performed at two transects distributed parallel and perpendicular, respectively, to the SDI line, during an irrigation event. The ERT results were compared to HYDRUS 2-D outputs and the relative differences were explained in the form of local heterogeneities in electrical resistivity (ER) changes, as a *proxy* for soil water content (SWC) variations. Concurrent simultaneous soil wetting and root water uptake during the last irrigation event of the season caused negligible changes in ER in the active root zone. Slight differences in ER were observed in the top 20 cm along the dripline, confirming that the emitter spacing is small enough to create a wetted strip along the processing tomato bed. These changes were also compared to SWC values measured with time domain reflectometry soil moisture sensors. A comparison between HYDRUS 2-D and ERT confirmed negligible changes in ER during irrigation due

* Corresponding author.
E-mail address: daniela.vanella@unict.it (D. Vanella).

https://doi.org/10.1016/j.scitotenv.2023.169620
Received 14 September 2023; Received in revised form 20 December 2023; Accepted 21 December 2023
Available online 28 December 2023

to simultaneous wetting and root water uptake processes. In addition, a good correlation was observed between the proximal sensed and the ERT results. Finally, the findings of this study underscore the necessity of using multiple methods for improving our knowledge of the SPAC system under real field conditions.

1. Introduction

There is an increasing need to improve the irrigation and nutrient use efficiency of major crops e.g., processing tomato in California's Central Valley (CDFA, 2021). Both for practical and research purposes, agricultural soils are generally monitored and sampled before, during, and after the growing season to establish water and nutrient balance (Lazcano et al., 2015). However, subsurface drip irrigation (SDI) and fertigation techniques increase the already heterogeneous water and nutrient distribution in the soil (Raij-Hoffman et al., 2022), making representative measurements a challenge under these complex cropping systems. In addition, the monitoring of the crop and soil water status as a *proxy* needs to be done for evaluating the correct application of water and nutrient and quantifying their effects on physiological processes. Thus, the need for implementing integrated monitoring approaches for monitoring the soil-plant-atmosphere *continuum* (SPAC) is pivotal.

A number of ground-based measurements are used for sensing both the soil and plant water status at point/local scale, including the use of portable sensors for detecting the crop water status parameters (e.g. stomatal conductance, photosynthesis, stem water potential, etc.) or measuring the soil water content (SWC, e.g., using probes based on time domain reflectometry, TDR, or frequency domain reflectometry method). Other methodologies are used for determining the energy and mass flux exchanges that act within the SPAC system at the field level (e.g., eddy covariance, or scintillometry techniques). In addition, the recent development in remote and proximal sensing technologies has provided useful data and tools for deriving spatially distributed information about the soil and plant system by combining the information captured by thermal, visible and near-infrared sensors at different temporal and spatial scales (including the use of water-related indexes, such as the normalized difference vegetation index, NDVI, Rouse et al., 1974; or the crop water stress index, CWSI, Idso, 1982; Jackson, 1982). Moreover, huge advances have been achieved in the quantification of the SWC in the root-zone.

In the last decades, hydrogeophysics (e.g., Binley et al., 2015), which involves the combination of geophysics and hydrological modelling, has provided promising approaches especially regarding the use of time-lapse applications for determining the spatial and temporal evolution of the SWC under herbaceous and woody crops (e.g., Cassiani et al., 2015; Garré et al., 2011; Michot et al., 2003; Moreno et al., 2015; Srayeddin and Doussan, 2009). In addition, the study of Vanella et al. (2019) opened an exciting research line on the integration of multiscale methodologies (i.e., by combining the use of remote sensing, modelling and geophysical methods) for supporting the irrigation management at the farm scale under drip irrigation conditions. The most advanced trends on precision agriculture coincide on the idea that applying integrated approaches, based on multiple monitoring/modelling techniques, can improve our knowledge of soil water redistribution under real field conditions (e.g., Heydari et al., 2023; Tsoulias et al., 2020).

At the light of the above-mentioned state-of-the-art, the specific objectives of this study were two-fold: (*i*) to infer the SWC redistribution and root water uptake processes during an irrigation event under subsurface drip irrigation in a processing tomato field using point-based sensors, hydrologic modelling and geophysical techniques; and (*ii*) to explore the potentialities of applying minimally invasive (i.e., ERT in time-lapse mode) and proximal sensing techniques (i.e., thermal and visible-near infrared information) for detecting the CWSI and SWC relationships under the experimental conditions.

2. Materials and methods

2.1. Field site description

The trial was conducted in a 34-ha commercial processing tomato field located in Yolo County, California (USA). The soil at the field site is defined as a Capay silty clay (https://casoilresource.lawr.ucdavis.edu/gmap/). Processing tomatoes were planted on April 6th 2021, and supplied by SDI with fertigation according to best management practices at the growers' discretion. The SDI dripline was buried in the middle of the growing bed at 20 cm depth, with a dripper spacing of 30 cm and a dripper discharge rate of 0.6 l h^{-1} (Fig. 1-A).

Irrigation was monitored using pressure transducers installed at the head of each irrigation line. The trial was performed on August 4th 2021, 20 days before harvest, during the last irrigation event for the growing season. At this phenological stage, the plants were mature, with fully developed canopies and root systems.

The SWC was monitored using 6 TDR sensors (TDR-3010H, Acclima, Inc., Meridian, USA) installed at the locations relative to the subsurface drip line, as described in Fig. 1-A at a distance of 35 m East of the ERT transects. Volumetric water content (VWC), soil temperature, and soil bulk electrical conductivity (EC) were recorded every 15 min during the ERT campaign (Table 1). Soil pore water EC in the root zone was calculated using TDR data according to the methodology presented by Hilhorst, 2000 Additionally, soil pore water EC was measured below the root zone, at 160 and 262 cm depth from the soil surface, using a deep vadose zone monitoring system as described in Rimon et al. (2007).

2.2. ERT setup and data processing

Electrical resistivity tomography (ERT) measurements were performed using a 10-channel Syscal Pro georesistivimeter (IRIS Instrument, Orleans, France) in a time-lapse mode. Specifically, one ERT dataset was acquired early in the morning, before the irrigation event (T0), and then, after the beginning of the irrigation phase (irrigation phase started at 10:23 AM PST), 7 subsequent ERT datasets were acquired at a nearly hourly rate until 5:00 PM during the irrigation event (T1–T7, Table 1).

Two ERT transects were arranged with a bi-dimensional (2-D) scheme, one perpendicular and one parallel to the growing beds (Fig. 1-B). The perpendicular ERT transect had 48 electrodes (stainless steel rods of about 0.30 m, with a diameter of 0.01 m, buried for about 1/3 of their length into the soil surface) spaced 15 cm, covering 4 beds or 7.1 m (ERT-1 (a-a′) in Fig. 1-B). The parallel ERT transect had 32 electrodes spaced 10 cm, covering 3.1 m (ERT-2 (b-b′) in Fig. 1-B).

For both ERT transects, direct and reciprocal measurements were acquired using a dipole-dipole configuration by automatically switching the current electrodes with the potential electrodes. The measurement error of the ERT data was assessed by calculating the reciprocal error above 10 % (Slater et al., 2000). In this sense, we can exclude abrupt ER changes occurred within the acquisition process.

The forward and inverse solutions were obtained from the ERT data using the R2 code (v4.02, July 2020). The ERT-1 and ERT-2 soil domains were discretized by generating two triangular meshes, made of 4672 and 4756 cells, and 9040 and 9280 elements, for ERT-1 and ERT-2, respectively, using the Gmsh software (Geuzaine and Remacle, 2009). Several forward models were created for determining the model error. Both measurement and model errors were used into the inversion model that was performed in absolute and in time-lapse mode. In particular, the absolute inversion model was applied as defined in Binley and Kemna

(2005) and Binley et al. (2015) for determining the initial electrical resistivity (ER) distribution at T0 (Table 1) at each transect. The temporal ER changes (in percentage, %) were calculated using the ratio time-lapse inversion approach described in Vanella et al. (2021, 2022). This ratio time-lapse inversion approach permits to identify the increasing or decreasing patterns referring to the ER changes in comparison to the initial condition (T0, Table 1).

Due to the uncertainty of the actual subsurface dripper location, an optimization approach based on ERT data was developed to infer the dripper location at each soil bed monitored with ERT-1. It was hypothesized that the actual dripper location is within the soil wettest location (inferred by ERT) in each beds' profile following a significant time period after the beginning of the irrigation event. Specifically, an area of 40 cm by 20 cm was defined around the theoretical dripper location as described by the grower, with ±20 cm in the x axis and ± 10 cm in the y axis (Fig. A.3-A). Then, the locations characterized by the more accentuated ERT decreasing changes at T2, were selected as the potential subsurface dripper location. In particular, T2 was chosen, that corresponded to 49 min after the beginning of the irrigation event (Table 1), since T1 was initialized only 15 min after the irrigation began and the SWC changes at that time were still too low to find an optimum location.

2.3. Ancillary monitoring data

2.3.1. Micrometeorological data

Surface energy balance components, such as net radiation (Rn), soil heat flux (G), sensible heat flux (H), and latent heat flux (LE) (Fig. 2) (all measured in W m^{-2}), along with other agrometeorological parameters, such as air temperature (°C), relative humidity (%), and solar radiation (W m^{-2}), were continuously monitored using an eddy covariance (EC) station that was positioned close to the ERT transects.

The EC system included a three-dimensional (3-D) sonic anemometer (Gill R3-50, Li-Cor Inc., NE, USA) to measure the orthogonal wind velocities, and an open path gas analyzer (LI-7500, Li-Cor Inc., NE, USA), that was installed 2.5 m above the ground in order to measure both carbon dioxide and water vapor fluxes at a frequency of 10 Hz. Also, three soil heat flux plates (HFT-3, REBS Inc., WA, USA) were buried at 8 cm depth and coupled with soil moisture probes (GS-1, METER Group Inc., USA), and soil thermocouples (TCAV-L, Campbell Scientific Inc., UT, USA), placed at 2.5 cm depth to correct the heat storage above the plates. The flux data were then post-processed by applying several standard corrections and adjustments using the Eddy Pro software (Li-Cor Inc., NE, USA). For further information on the flux tower and data processing refer to Peddinti and Kisekka (2022).

Table 1
Time-lapse electrical resistivity tomography (ERT) measurements carried-out in a processing tomato field in Yolo County California during the 2021 growing season.

ERT time step	Irrigation conditions	Starting time (hh: mm)	Ending time (hh: mm)
T0	Without irrigation	8:33 AM	9:04 AM
T1	During irrigation	10:38 AM	11:07 AM
T2		11:12 AM	11:53 AM
T3		12:27 PM	12:56 PM
T4		1:21 PM	1:51 PM
T5		2:26 PM	3:06 PM
T6		3:58 PM	4:28 PM
T7		4:55 PM	5:25 PM

2.3.2. Thermal-based plant water status monitoring

Canopy temperature was monitored at different time steps, at the end of each ERT acquisition (Table 1) using a portable infrared radiometer (MI-220 model SI-121, Apogee Instruments, Inc., Logan, USA). The instrument was mounted on a pole and a fixed angle of 90° from the vertical and a 30 cm distance from the canopy was maintained during the measurements. At the ERT-1 transect, two measurements per growing bed were performed, one above each plant (Fig. 1). At the ERT-2 transect, it was not possible to identify individual plants, so canopy temperature measurements were performed every 30 cm or every 3 electrodes. At each measurement time step, the sky temperature data was also acquired and used to obtain the corrected canopy temperature values using the following Stefan-Boltzmann-based formula:

$$T_{Target} = \sqrt[4]{\frac{T_{Sensor}{}^4 - (1-\varepsilon) \bullet T_{Background}{}^4}{\varepsilon}} \quad (1)$$

where T_{target}, T_{sensor} and $T_{background}$ refer to the corrected, measured, and sky temperature (i.e., brightness temperature of the background), respectively; ε is the emissivity of the target surface, i.e., 0.98 for vegetation (Campbell and Diak, 2005).

The correct canopy temperature and air temperature (from the in-situ agrometeorological station) measurements were used to compute the CWSI during the ERT measurements, using the Idso (1982), Jackson (1982) equation as follows:

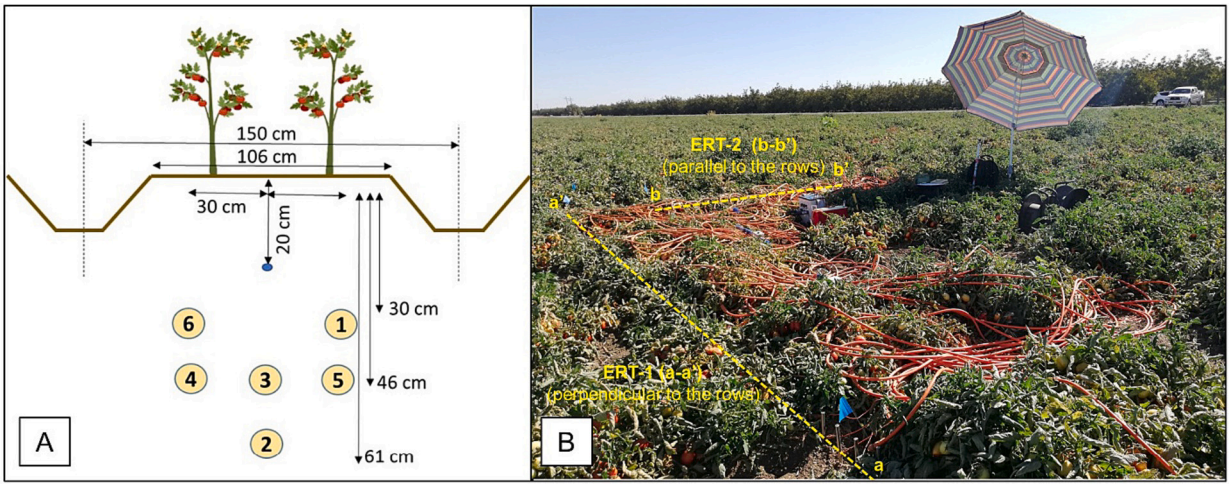

Fig. 1. (A) Layout of the tomato growing bed, subsurface drip irrigation line, and time domain reflectometry (TDR) sensor locations. The blue dot represents the location of the actual subsurface drip irrigation line. Circled numbers represent TDR sensors installed horizontally in the area near the electrical resistivity tomography (ERT) transects; (B) Overview of ERT transects, perpendicular and parallel to the growing beds (ERT-1 and ERT-2), respectively, at a processing tomato field in Yolo County California during the 2021 growing season.

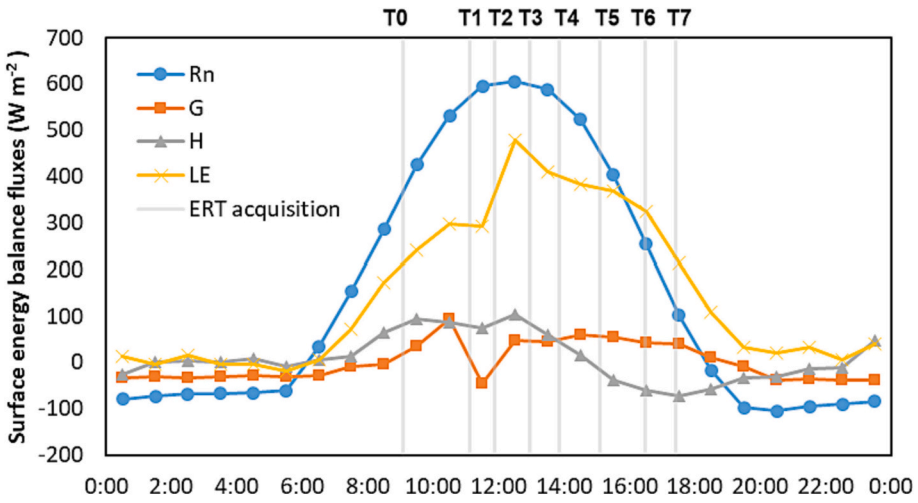

Fig. 2. Hourly surface energy balance fluxes measured in a processing tomato field in Yolo County California during the 2021 growing season. Timings of electrical resistivity tomography (ERT) acquisitions are reported as light vertical grey lines (T0–T7, Table 1).

$$CWSI = \frac{(T_c - T_a) - (T_c - T_a)_{LL}}{(T_c - T_a)_{UL} - (T_c - T_a)_{LL}} \quad (2)$$

where T_c and T_a refer to the canopy and air temperature (°C), respectively; LL and UL are the lower and upper limits, respectively.

The term $(T_c - T_a)_{LL}$ was determined on experimental basis by fitting the theoretical $(T_c - T_a)$ with the vapor pressure deficit (VPD) values measured in situ (kPa). This relationship resulted in the following equation:

$$(T_c - T_a)_{LL} = (-1.3133 * VPD) + 1.213 \quad (3)$$

The $(T_c - T_a)_{UL}$ was calculated using three different temperature values provided at the site-specific condition (i.e., 8 °C), and reported by Irmak et al. (2000) (i.e., 4.6 °C) and López-López et al. (2009, 2011) (i.e., 2.8 °C) for herbaceous crops.

2.3.3. Aerial imagery data

A day before the ERT campaign, very high-resolution aerial imagery was taken using an airplane by CERES (Ceres Imaging, Inc., CA, USA). This imagery included multispectral images with a pixel resolution of 0.3 m and thermal images with a resolution of 0.2 m. The images were captured at 12:55 p.m. (PST) using the thermal sensor FLIR A65 (FLIR Systems, Wilsonville, Oregon, United States) in conjunction with a bespoke arrangement of a constellation of VNIR IDS camera systems. Readers can refer to Peddinti and Kisekka (2022) for additional information on image processing and acquisition processes. These images were utilized in the calculation of the NDVI as a *proxy* for the vigor of the vegetation (Rouse et al., 1974), and the NDVI values were extracted for each of the electrode locations of both ERT-1 and ERT-2. After that, these NDVI values were compared with the relative ER changes that occurred during the course of a day. The ER values between two neighboring electrodes in the ERT sections were averaged for each of the depths. To prevent the boundary effects from occurring, the first and last six data points were ignored as well as the points inside the furrow in ERT-1.

2.4. Hydrological simulations

Unsaturated soil water flow was simulated using HYDRUS (2-D/3-D) software, version 2.05.0270, following a modified Richards equation and using van Genuchten (1980) – Mualem (1976) hydraulic functions (Šimůnek et al., 2011). For additional details on SDI modelling using HYDRUS (2-D/3-D), the reader is referred to Raij-Hoffman et al. (2022).

2.4.1. Domain and hydraulic properties

A 2-D domain was defined following the simulations in Raij-Hoffman et al. (2022) and the growing bed geometry defined in Fig. 3 with a profile depth of 150 cm. Assuming geometrical bed symmetry, the simulation included half of the growing bed for computational efficiency. The water flow domain was defined with a subsurface dripper and a finer discretization around the dripper and at the top boundary

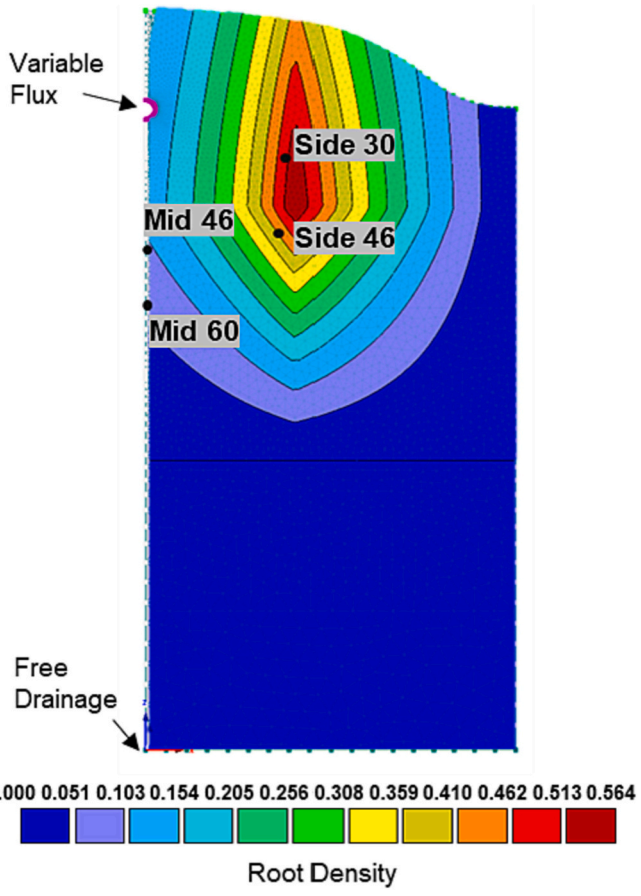

Fig. 3. HYDRUS 2-D/3-D modelling domain for subsurface drip irrigation, root density distribution and boundary conditions. Observation points represented as black dots at the locations where the time domain reflectometry (TDR) sensors were installed.

resulting in 3951 nodes and 3667 elements.

Hydraulic properties were estimated using the Rosetta3 pedotransfer model with measured inputs of sand, silt, and clay percentages as well as bulk density measured in the top 30 cm of soil (Table 2). In particular, soil texture and bulk density were measured at 4 different locations in this field at depths of 0–15 cm, 15–30 and 30–60 cm using a modified pipette method (Waterhouse et al., 2021) and the gravimetric method, respectively. The results of the soil analyses showed low spatial heterogeneity and no clear difference between the cultivated layer and the deeper soil. Due to the low vertical heterogeneity also inferred by ERT at the beginning of the field campaign (T0, Table 1, refer to Fig. 4), it was decided to assume vertical homogeneity and use the top 30 cm properties for the entire soil profile.

In order to account for the natural spatial heterogeneity, fifty simulations were generated with stochastic distributions of the hydraulic conductivity (αK) and pressure head (αh) scaling factors using the Miller-Miller similitude approximation (Miller and Miller, 1956), where these two scaling factors are correlated. The mean Ks for the stochastic distribution is presented in Table 2, the standard deviation of log10 value of αK was defined as 0.25 cm, and zero as horizontal (X) and vertical (Z) correlation lengths (uncorrelated in any direction).

Root density was defined using the Vrugt model (Vrugt et al., 2001) with a maximum rooting depth of 90 cm, depth of maximum intensity of 40 cm, a shape empirical parameter Pz[−] of 2, maximum rooting radius of 75 cm, radius of maximum intensity of 30 cm and a shape empirical parameter Px[−] of 5, indicating that the plant is not on top of the dripper at x = 0 cm, but at the side of the drip line (Fig. 3) following the agricultural practice in the field and experimental measurements conducted in similar but not identical cases (Hanson and May, 2007).

The Feddes water uptake reduction model (Feddes et al., 1978) was considered with h_1, h_2, h_{3max}, h_{3min}, h_4 values of −1, −2, −800, −1500, and −8000 cm, respectively, as described in Hanson et al. (2006) and a critical stress index of 0.8 assumed to allow for compensated root water uptake. No solute stress model was included in the simulation, and overall, no water uptake reduction due to low water content or salinity was expected, since irrigation was scheduled to be sufficient in volume and performed with low-salinity water.

Four observation points were defined at the 4 relative locations of the TDR sensors (Figs. 1-A and 3), assuming total symmetry, and therefore sensor pairs located at the same depth and distance from the dripper are represented as one observation point. These are sensors 1–6 and 4–5 in Fig. 1-A.

2.4.2. Initial and boundary conditions

Following Raij-Hoffman et al. (2022), the boundary condition at the dripper was defined as a variable flux, allowing for intermittent irrigation, and the bottom boundary was defined as free drainage (Fig. 3). The rest of the domain was defined as no flow assuming symmetry on both sides of the profile and all ET to be transpiration due to the high plant cover during the field campaign and the extremely dry bare soil areas due to the subsurface drip irrigation system.

The irrigation rates applied in the field and the actual hourly ET measured with the EC method were defined as time variable boundary conditions (as in Groenveld et al., 2021). The typical irrigation strategy followed by the farmer (i.e. long duration events) lead to assume that actual ET provided by the EC is quite close to potential crop ET (i.e. no stress conditions). The initial conditions were defined as a uniform VWC of 0.36 cm^3 cm^{-3} as estimated from the initial ERT dataset (T0, Appendix B, Figs. B.1.-B and B.2.-B).

3. Results

3.1. Time-lapse electrical resistivity images

The ER pattern at T0, before the irrigation event begun, in Fig. 4. suggests lower SWC and in the shallow profile as a result of evaporation and root water uptake, as well as some water storage in the deeper parts of the profile (70 cm).

The perpendicular profile (ERT-1, Fig. 4a) shows higher ER values in the furrow area than in the plant area, suggesting that the furrow acts like a hydraulic barrier without water flow or root water uptake for subsurface drip irrigation. Furthermore, most of the patterns described in Fig. 4 are due to small differences in ER and only discernible when looking at the data log-transformed, therefore supporting the assumption that the soil profile is relatively uniform in absolute terms (24 h after the last irrigation event ended, Table 1). The ER patterns that are visible with the untransformed data are: (*i*) the higher ER values in the edges of the growing beds may be due to soil surface exposures of the edges, i.e., no crops covered the edges resulting in soil drier conditions due to the higher soil evaporation, and/or to geometry differences from the theoretical profile used to create the mesh for the ERT analysis; and (*ii*) the higher ER values in the top 20 cm on the right side of the ERT-2 profile, probably due to the higher roots density.

Referring to the time-lapse results at ERT-1, during the irrigation event, the ER increased between the growing beds and decreased around the subsurface dripper line (between the two crops, where a lower root density is expected), suggesting the homogenous distribution of the irrigation water around the drippers and the simultaneous root water uptake patterns occurred on both sides of the bed, where the two tomato plants were located (Fig. 5). Note that the theoretical and the recognized optimized subsurface dripper locations at ERT-1 (Fig. A.1.-A) are shown also in Fig. 5 referring to the different monitored time-steps.

In the parallel direction to the drip line (ERT-2), lower ER changes were observed during the irrigation event, suggesting simultaneous wetting and root water uptake processes in the root zone (Fig. 6). Areas with no change in ER during the ERT campaign, represented in white in Figs. 5 and 6, suggest areas where root water uptake was equal to the water addition from the irrigation and, therefore, no changes can be seen during the monitoring time period. These areas are identified on the sides of the drippers on the perpendicular transect (ERT-1) and at around 20 cm depth in the parallel transect (ERT-2). In addition, there are areas below the furrow with no changes, suggesting negligible root water uptake or water distribution processes.

The distribution of the overall ER changes (%) during the monitored time steps (T1–T7, Table 1) of the irrigation phase in reference to the initial condition (T0, no irrigation) for ERT-1 and ERT-2 transect, respectively, is given in Fig. A.2.-A.

3.2. Soil-plant atmosphere continuum monitoring

During the experiment, the irrigation began at 10:30 in the morning, which was approximately 210 min after the first data set (T0) was collected (Fig. 7).

The ET values began to increase around 7:30 AM prior to irrigation,

Table 2
Soil texture, bulk density and soil hydraulic parameters estimated using Rosetta3 pedotransfer function and used in the HYDRUS (2-D/3-D) simulations. θr is the residual VWC, θs is the saturated VWC, *α* and n are empirical parameters related to the inverse of the air entry pressure and the pore-size distribution, respectively and Ks is the saturated hydraulic conductivity.

Sand (%)	Silt (%)	Clay (%)	Bulk density ($g\ cm^{-3}$)	θr ($cm\ cm^{-3}$)	θs ($cm^3\ cm^{-3}$)	α ($1\ cm^{-1}$)	n (−)	Ks ($cm\ h^{-1}$)
24.03	37.25	38.72	1.41	0.115	0.44	0.007	1.33	0.397

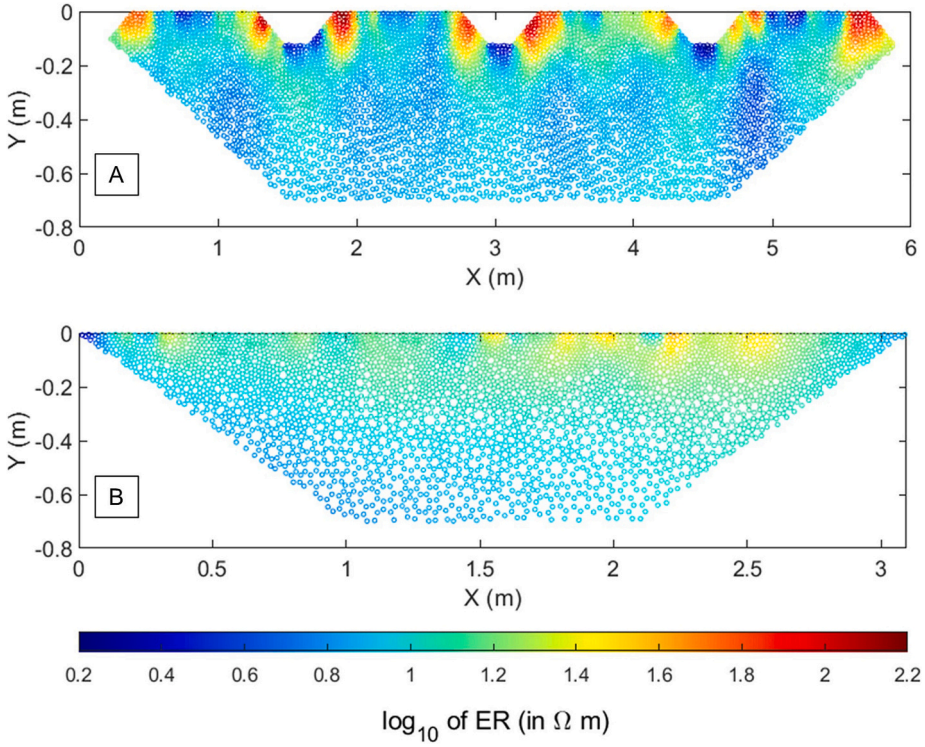

Fig. 4. Absolute resistivity values for (a) ERT-1 and (b) ERT-2 transects before the irrigation event in a processing tomato field in Yolo County California during the 2021 growing season. Values are expressed in log10 of the electrical resistivity (ER) in Ω m.

and they reached their highest point at 14.00 PM, which is when the T4 ERT data set was recorded (Fig. 2). Later on, the ET values continued to go down, and by the time the last data set was collected (T7), the ET values had hit 0.3 mm/h. After that, they went down until they reached zero by the end of the day (which was at 18:00 PM). Over the entirety of the time period, the rates of irrigation were greater than the rates of tree transpiration.

SWC measured by the TDRs installed in the middle of the row showed a gradual decrease in VWC during the first part of the day (Fig. 7). At 46 cm depth, the SWC began to increase when the inputs (irrigation amount) became larger than the output (ET fluxes), showing evidence of simultaneous wetting and drying processes until then, reducing any observable changes in either SWC or ER in the soil. At 61 cm depth, the SWC increased sharply at 9:30 PM (Fig. 7).

Soil temperature fluctuations during the ERT campaign were observed only at 30 cm, while deeper sensors showed no change. Relative soil temperature changes (*RelT*, Fig. A.3.-A) were calculated with Eq. (4), where T_i is the temperature at T0 and T is the temperature at each time step:

$$RelT = \left(\frac{T}{T_i} - 1\right) * 100 \quad (4)$$

These fluctuations were less than 1 °C and a total of up to 2 % of the soil temperature at the beginning of the ERT campaign. Relative soil pore water EC changes, estimated using TDR data, were also up to 2 % from the soil pore water EC at T0 (Fig. A.3.-A). Deeper soil solution measurements at 1.60 and 2.62 m showed stable soil pore water EC of about 1 dS/m before, during and after the ERT campaign,

3.2.1. Crop water status determinations

The CWSI resulted in similar average values ranging from 0.31 to 0.47 and from 0.27 to 0.41 at ERT-1 and ERT-2, respectively, using different $(T_c - T_a)_{UL}$ baselines (i.e. 8 °C, 4.6 °C and 2.8 °C for the site-specific conditions), and as reported by Irmak et al. (2000) and López-López et al. (2009, 2011). The temporal evolution of the CWSI, using these upper baselines, during the time-lapse ERT surveys (ERT-1 and ERT-2) is given in Fig. A.4-A.

Fig. A.4-A. shows similar CWSI increasing trend in accordance with the atmospheric water demand and irrigation application. In particular, lower CSWI values were obtained early in the morning and after 7 h since the beginning of the irrigation phase; whereas, higher values were observed in the hottest hours of the day (Fig. 3). In absolute terms, similar values were obtained for the CWSI formulations obtained with the local upper baseline and the value provided by López-López et al. (2009, 2011). A strong relationship was observed between the average ER changes (%) and CWSI obtained in time under the site-specific condition at ERT-1 ($R^2 = 0.83$); whereas a weak relationship was achieved for ERT-2 (Fig. A.5.-A).

3.2.2. Relationships between soil and plant interactions

At T0, before the irrigation started, there was a negative correlation between longitudinal ER in ERT-2 and NDVI (Fig. A.6.-A). This could evidence that even though higher biomass will result in higher transpiration, it will also result in higher soil water depletion and lower evaporation, therefore causing higher VWC (and therefore lower ER) two days after the last irrigation in areas with healthier vegetation.

At the end of the ERT campaign at T7, i.e., 7 h after the irrigation started and almost at the maximum cumulative daily ET (Fig. 7), there is a positive correlation between ERT-2 change and NDVI, suggesting a lower SWC for higher NDVI locations and an evidence of higher biomass transpiring more water during a combined irrigation and ET event (Fig. A.6.-A). Even though the correlations between ER and NDVI in ERT-1 are weaker than for ERT-2, they still show the same trend. This weaker relationship in ERT-1 could be explained by the less crop vigorousness (and even the presence of bare soil) in this transect, which results in a higher NDVI range (0.30–0.70 versus 0.62–0.74 for ERT-2 and ERT-1, respectively), hindering the possible relationship between crop NDVI and the correspondent ER (and ER change) (Fig. A.6.-A).

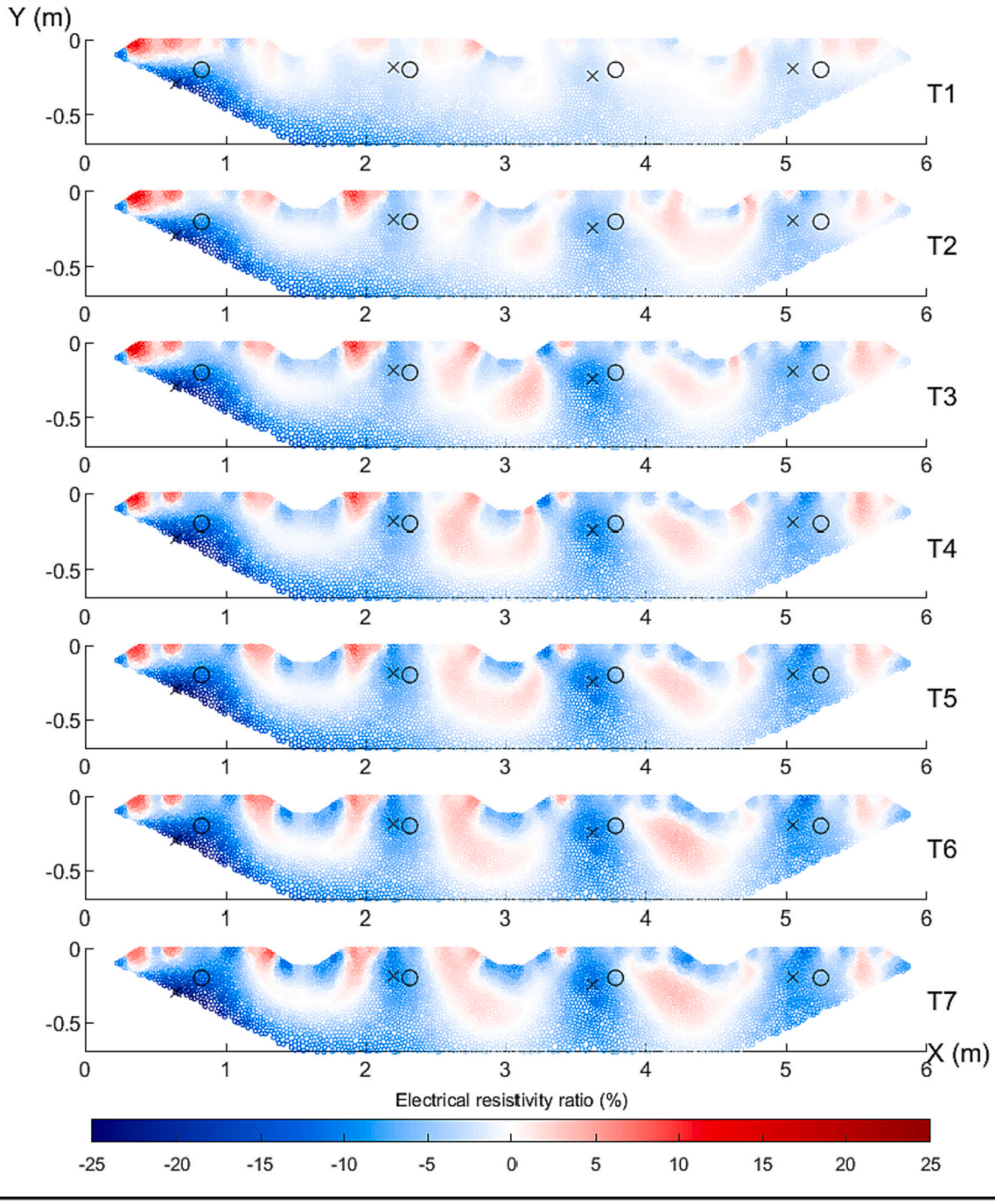

Fig. 5. Electrical resistivity changes (ER, ratio %) during different time steps (T1–T7, Table 1) of the irrigation phase in reference to the initial condition (T0, no irrigation) for ERT-1 transect. Theoretical dripper location marked with circles and optimized dripper location marked with "x".

3.3. Hydrological simulations

Simulated and measured VWC decreased during the beginning of the irrigation event, following the measured trends in the soil water balance, with the cumulative ET becoming higher than the cumulative irrigation at 2:30 PM (T5, Table 1, Figs. 7, 8). About an hour after T5, there was an increase in measured and modeled VWC at 26 cm below the drip line (Fig. 8-B – 46 cm mid), followed by a slight increase in the VWC at 30 cm below ground level and at a lateral distance of 30 cm from the middle of the growing bed and drip line around 5:00 PM (Fig. 8-A).

The TDR sensors and observation points at 46 cm below the soil surface level and a lateral distance of 30 cm from the middle of the growing bed showed a slight increase of VWC after 8:00 PM (Fig. 8-B). At the same time, a sharper VWC increase was observed by the TDR at 40 cm below the drip line, while the model showed a more moderate increase in VWC (Fig. 8-C). The model and measured were not calibrated to match one-to-one, but homogeneous soil properties were used to simulate the general trends. The profile is assumed to be symmetrical by design, however, two TDRs located in the same relative position showed the same relative SWC changes with a consistent lag of 0.02 cm^3cm^{-3} and a model that will be calibrated to one of the TDRs will not agree with the other side of the measurements. An example of the effect of this assumption can be observed in the evolution of TDR 30–46 series (each series corresponds to a different side of the bed) (Fig. 8). In general, both series followed the same pattern, with few points not falling in the general trend. These discrepancies represent a limitation of the model,

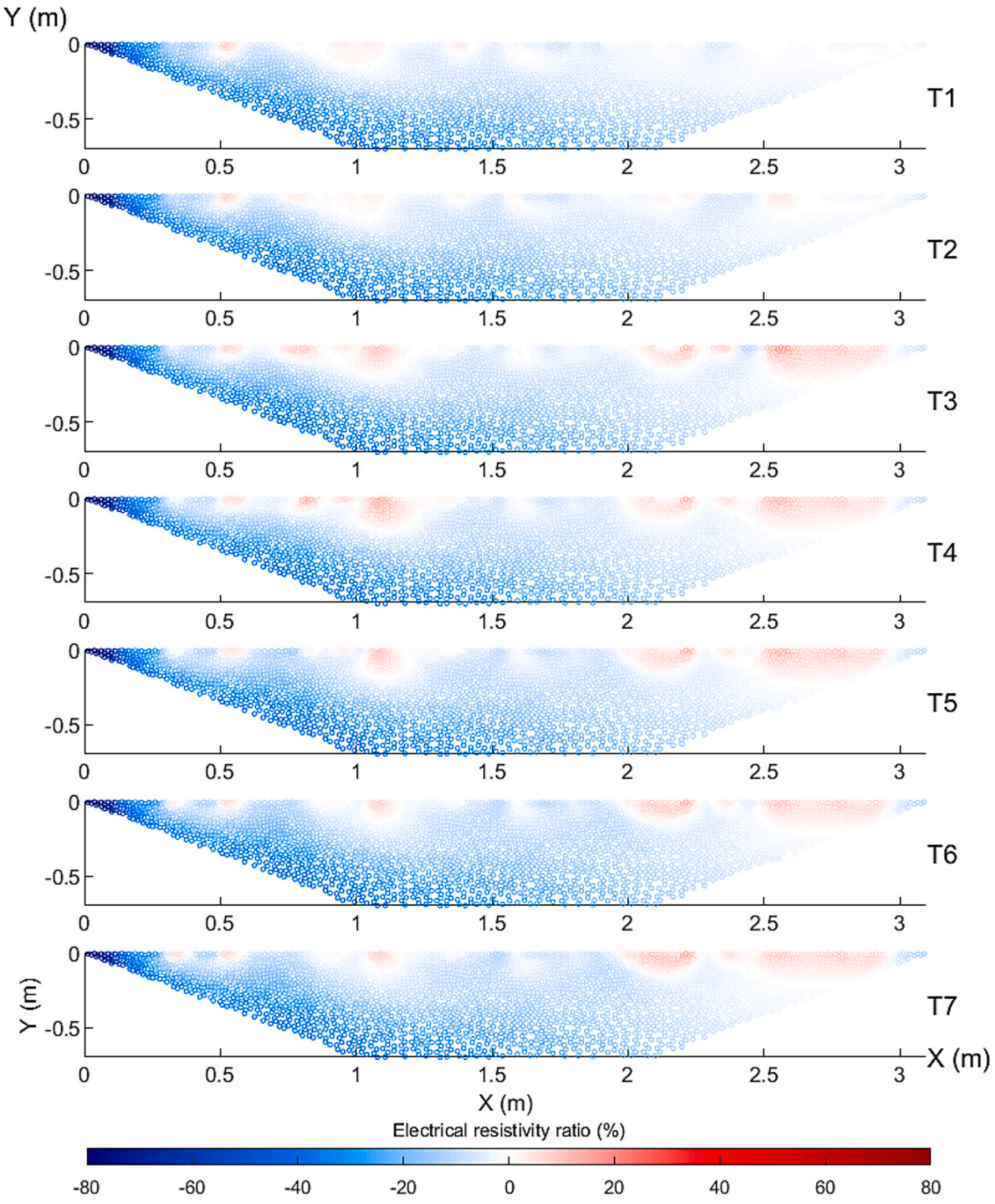

Fig. 6. Electrical resistivity changes (ER, ratio %) during different time steps (T1–T7, Table 1) of the irrigation phase in reference to the initial condition (T0, no irrigation) for ERT-2 transect. Theoretical dripper location marked with circles and optimized dripper location marked with "x".

and evidence some uncertainties of the model (e.g., irrigation line misalignment, heterogeneity of root distribution among different crops).

Both ERT and model capture the general shape and trends (Fig. 9). While the simulations assume symmetry of the soil profile, the changes in ER during the irrigation event provided with an opportunity to observe the relative changes at replications of the simulated half profile. The two central beds from the monitored area during the ERT campaign (Fig. 1-B) were segmented into 4-half growing beds representing the simulated profile (Fig. 9). The profiles were segmented vertically at the optimized dripper location (x in Fig. 9) and TDR locations relative to the optimized dripper. The relative changes in ER can be visually compared to relative SWC changes in the HYDRUS (2-D/3-D) simulations. In both the model and ERT measurements it can be observed that there are negligible changes in either SWC or ER in the observation nodes located to the side of the dripper until T4. These modeled and measured results are in agreement with the observed higher ET than irrigation until 2:30 PM (T5). Areas of decrease in SWC and increase in ER are observed as expected in the middle of the profile, where plants are located. Even though a clear wetting front profile is observed in the simulations, with a symmetrical circle around the dripper as expected in a clay loam soil, this theoretical pattern is not observed in the ERT change data (Fig. 9).

4. Discussion

In this study, a combination among multi-dimensional minimally invasive techniques (i.e., geophysical and proximal sensing-based

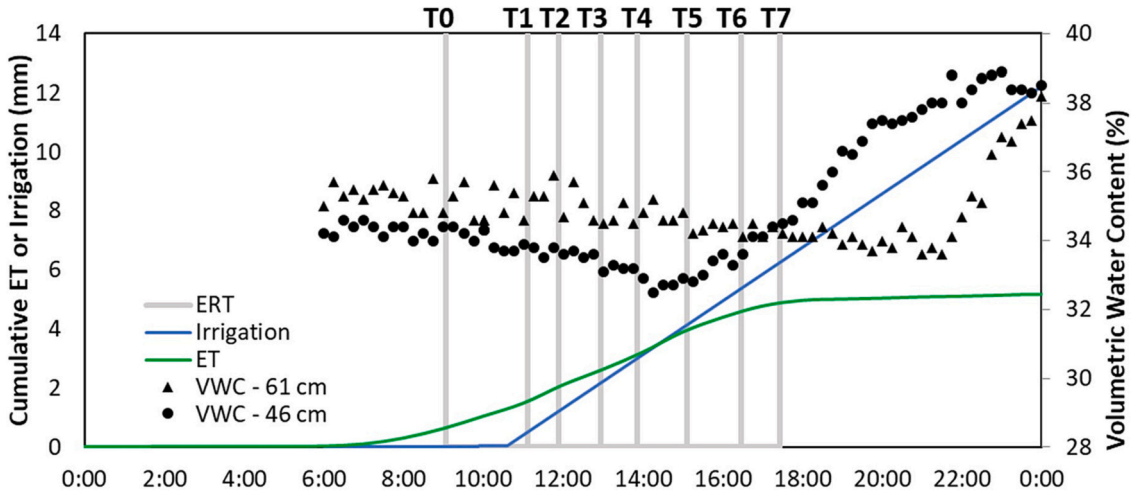

Fig. 7. Volumetric water contents (VWC) at 46 and 61 cm depth (circles and triangles, respectively) and timing of each ERT acquisition in grey lines (T0–T7, Table 1) and cumulative measured evapotranspiration (ET) and irrigation during the electrical resistivity tomography (ERT) campaign (green and blue line, respectively).

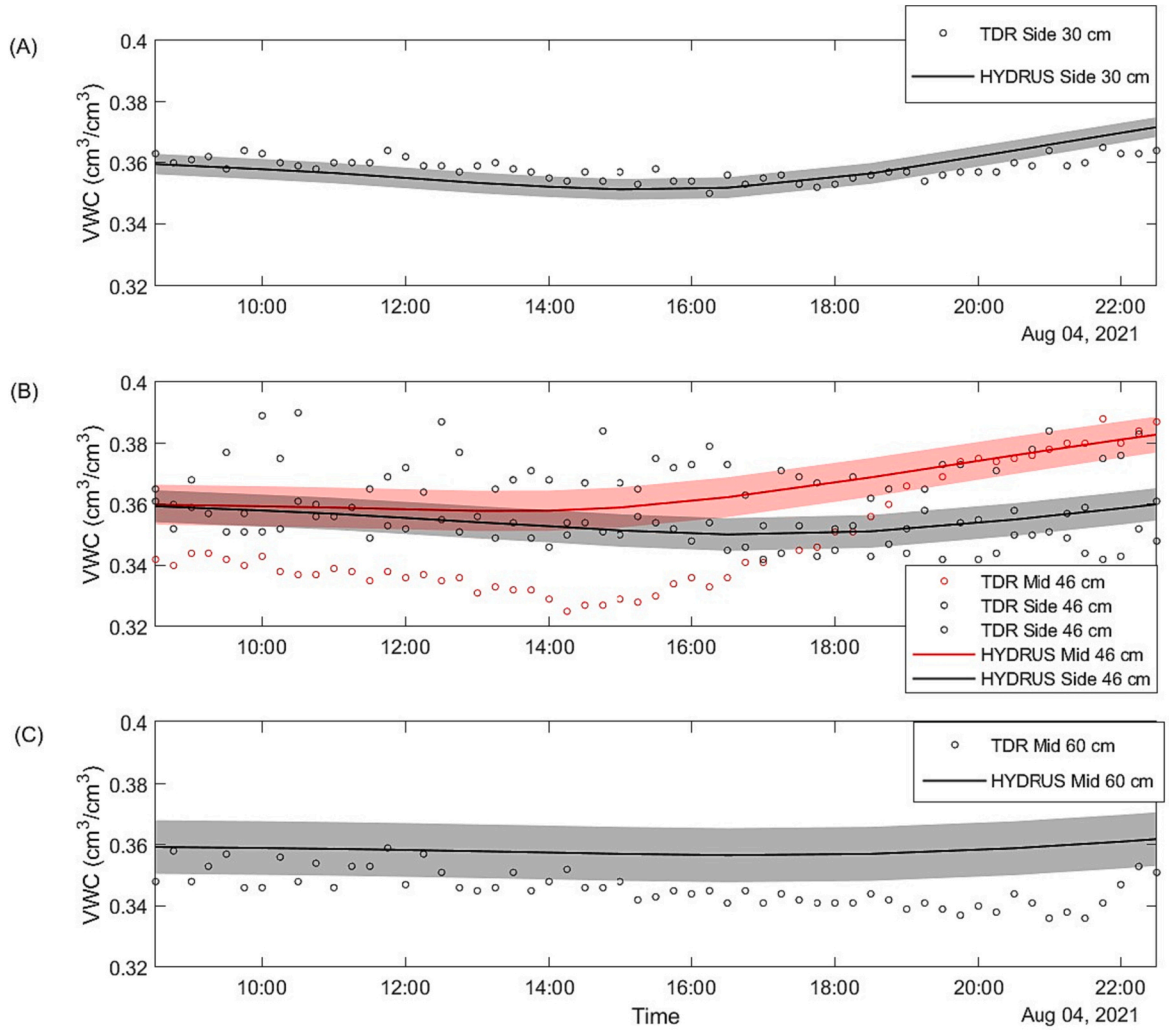

Fig. 8. Volumetric water content (VWC) simulated with HYDRUS 2-D/3-D and measured with time domain reflectometry (TDR) sensors during the electrical resistivity tomography (ERT) campaign, for four locations relative to the subsurface dripper in a processing tomato field in Yolo County California during the 2021 growing season. Shaded areas represent the 95 % confidence interval for the 50 simulations with stochastic distributions of the hydraulic conductivity and pressure heads.

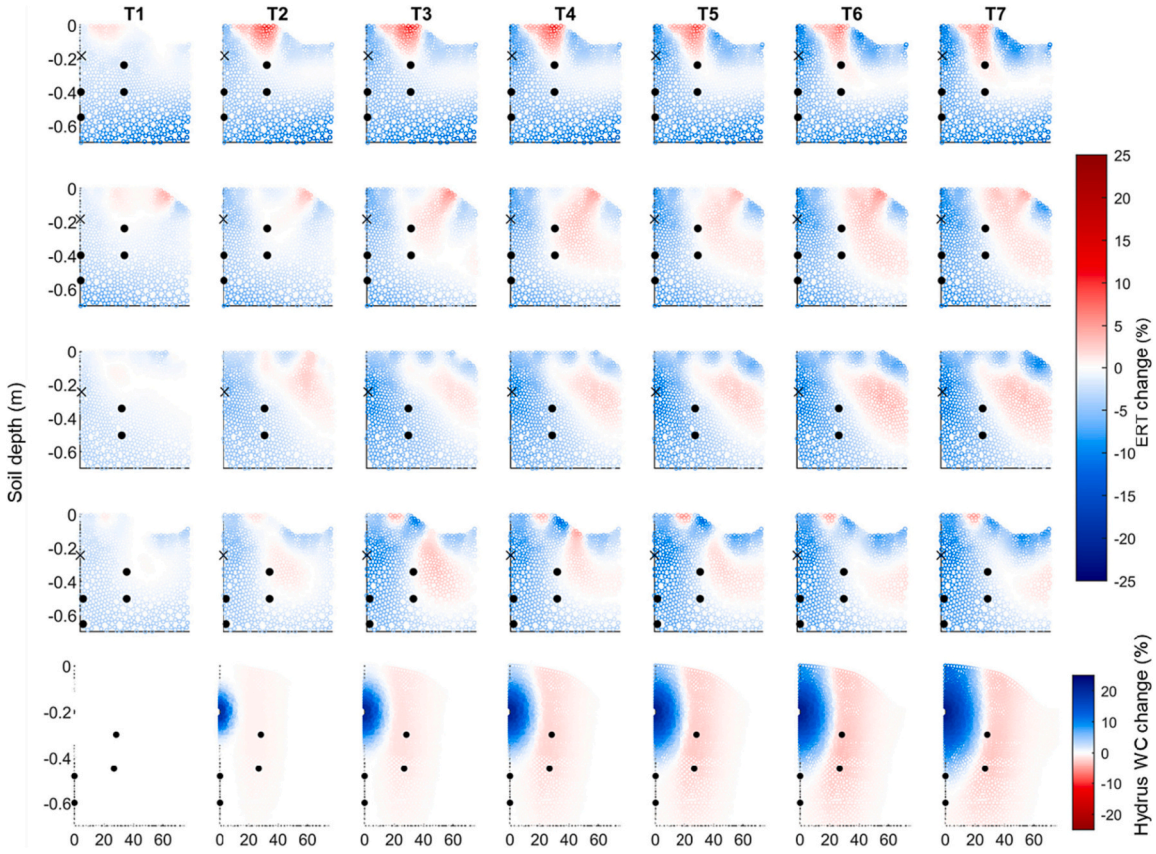

Fig. 9. Side by side comparison of relative water content changes during the electrical resistivity tomography (ERT) acquisition events as simulated by HYDRUS 2-D (bottom panel) and relative ERT changes (%) in the 4 upper profiles, each one half a bed as simulated in HYDRUS, assuming symmetry at the drip line location and in the middle of the furrow. Black dots represent time domain reflectometry (TDR) sensors locations relative to the dripper (x in the ERT graphs).

measurements) and hydrological modelling has provided site-specific information on soil water distribution and its interactions with crop features in a subsurface drip irrigated processing tomato field. Specifically, the results of this study highlight the practical role of the time-lapse geo-electrical approach for supporting the precision irrigation management (Vanella et al., 2021, 2022, 2023), and providing new insights to identify the subsurface dripper location. Specifically, this study promotes the use of relative ER changes as a *proxy* of SWC changes, being known that the absolute translation of ER into SWC is prone to additional uncertainty (does not deepen in this study; refer to Chen and Niu, 2022; Tso et al., 2019). Moreover, the potential of our findings is enhanced when the ERT surveys are applied in combination with other SPAC measurements (i.e., micrometeorological, multispectral and thermal information, and TDR sensors). Note that each available SPAC monitoring/modelling method may suffer from specific limitations, e.g., the scale of applications or the resolutions, that in some cases may be overcome with the advantages associated with the adoption of multiple methods (e.g., point-based measurements versus spatially distributed information). As a practical recommendation, the selection of the optimal approach depends on the desired target, the available costs (such as for the instrumentation and labor) and the response time in terms of data processing duration.

Herein, the inferred SWC changes by ERT were highly linked with the root water uptake as evidenced by the multispectral and thermal sensed crop monitoring responses. As example, a direct relationship was obtained between the CWSI and changes in ER (Fig. A.6.-A); showing higher ER changes (suggesting lower SWC), when CWSI increases as well. These results show the potential of time-lapse ERT in describing the CWSI within an irrigation event (Garré et al., 2011). Moreover, in our research conditions, the aerial-based NDVI patterns resulted inversely correlated with the absolute ER values acquired before the irrigation event (T0), suggesting higher soil water depletion in areas with higher plant biomass (Fig. A.8). Similarly, the NDVI was directly correlated to the ER changes at the end of the ERT survey, proposing that areas with higher plant biomass had more water removed from the soil during the day, than areas with lower NDVI. These findings are supported by visual-based observations conducted in the field. This is also in agreement with other studies that linked the crop features (e.g., detected by multispectral or other plant-based methods) with the ER-inferred SWC information (e.g., Brillante et al., 2015; Cassiani et al., 2015; Rossi et al., 2018; Vanella et al., 2018). No clear root water uptake patters were depicted in ERT-2, where some areas with an increase in ER, with time were identified as zones with lower NDVI, suggesting lower canopy density and, therefore, higher soil evaporation, probably related to plant establishment after transplanting (Vanella et al., 2023).

Interesting insights have been provided when ERT, hydrological modelling and ground-based soil moisture measurements using TDR were compared. Specifically, the comparison of TDR and HYDRUS-derived SWC values showed high accuracies at 30 cm and 60 cm, whereas higher discrepancies occurred at 46 cm positions (Fig. 8). These higher discrepancies are probably due to the fact that, when setting the initial modelling conditions, i.e., the root density, it was considered only one half of the bed (i.e. one plant). However, it is expected that at the center of the bed, an overlapping between the root system of the two crops occur, resulting in a hypothetically higher root density. This higher root density would result in a lower modeled SWC, being this decrement more evident at "46 cm Side" position. Thus, if this overlapping would have been considered, it is expected that the values modeled by HYDRUS and the ones provided by TDR had been more similar to each other. In general, faster soil water infiltration was

observed at ERT-,1 than modeled or measured with TDR sensors (Fig. 8). Also, ERT-2 showed greater vertical water redistribution after the beginning of the irrigation event. While clear wetting bulbs were visually identified in ERT-1, the results obtained at ERT-2 confirms the assumption that the soil water distribution along the subsurface drip irrigation line is close enough to create a linear wetting pattern in the direction along the line instead of radial water distribution (Figs. 5 and 6). Vanella et al. (2021) have already highlighted the potential of time-lapse ERT monitoring in depicting the shapes of the wetting bulbs. In addition, in relative terms the variability between the relative TDR locations in the ERT repetitions along the ERT-1 transect was lower and averaged ~2 % (Appendix B).

In general, the variability in the ER profiles decreased with depth in both transects (Figs. 5, 6, A.2.-A, C.1.-C and C.3.-C). This behavior is in agreement with the hydrological modeled results (Figs. 9, C.2.-C) and with previous ERT-based studies that found that the maximum root mass distribution is mainly located in the shallow subsoil for herbaceous crops (e.g., Amato et al., 2008). Moreover, even if the ER variability decreased with time, the SWC values increased. The assumption is that the ER values at the beginning of the simulation, when the soil is expected to be drier, may be influenced by other factors, such as soil texture, salinity, even soil temperature. Then, when the irrigation begins and water redistributes, the SWC becomes the factor of highest influence on ER changes, and, therefore, acts as a homogenizing factor for ER. As well-known, the soil ER is dependent on several parameters referring both to the static and state proprieties of the soil (Samouëlian et al., 2005). In this study, we applied the ratio inversion ER time-lapse approach in order to minimize the contributions of these multiple variables on soil ER and addressing the ER change for the most to the SWC changes. In particular, note also that, the time-lapse ERT surveys were carried out at the same locations (ERT-1 and ERT-2) and during the ERT acquisitions the soil temperature and EC of the soil pore solution changes were lower than 2 %, thus, the soil temperature and salinity effect on ER was ignored. On the other hand, the HYDRUS 2-D/3-D domain is either (i) completely ideally homogeneous with the only factor influencing the variability being the SWC redistribution, as a consequence of irrigation-water and root uptake-water flow or (ii) characterized by a theoretical heterogeneity as presented in this work. As example, the comparison between ERT and HYDRUS evidenced that water is moving down faster than how is modeled by HYDRUS, suggesting a limitation of the use of models for this kind of analysis, especially the critical role that the setting of the initial conditions has on the final obtained results. Thus, the initial variability observed in terms of ER, together with the related inversion uncertainty, can be used to set-up site-specific hydrological domains using integrated approaches (Rao et al., 2020, Tso et al., 2020) also based on coupled numerical models and/or data assimilation methods (Mary et al., 2021).

5. Conclusions

This study represents an attempt to approach the soil water dynamics monitoring from a multi-perspective point-of-view. Of course, this is a complex challenge and herein we do not have the claim to propose an integrated SPAC monitoring approach, but at least to present the potential of using several stand-alone monitoring methods to describe the main soil-plant interactions under subsurface irrigation context. In this sense, multiple 2-D time-lapse ERT measurements, carried out in transects in perpendicular (ERT-1) and parallel (ERT-2) to the subsurface drip irrigation line, provided in-situ insights of water redistribution, resulting in concurrent soil wetting and drying patterns, because of simultaneous irrigation and root water uptake processes in a tomato field. Moreover, the ERT design applied in the present study allowed us to evaluate the ER distribution in the third dimension not considered in each single transect in a pseudo 3D manner. In particular, slight ER increases were observed in in the active root zone on the sides of the dripper in ERT-1 and in the top 20 cm in ERT-2, whereas close to the drippers, an ER decrease occurred both in ERT-1 and ERT-2. Thus, the two ERT transects showed different potentialities, being ERT-1 more useful for defining the lateral expansion of the wet bulbs, whereas ERT-2 allowed evaluating the performance of the irrigation system (e.g. dripper clogging would result in an increase of ER).

Moreover, the use of ancillary data acquired by proximal sensing techniques, such as CWSI and NDVI, has evidenced of how the crop water status processes affected the soil dynamics inferred by ERT and vice versa.

The ERT measurements permitted to depict the high spatial variability of the SWC distribution as derived from the different TDR-based observation points located in symmetrical locations from the drip line. Therefore, it was not realistic or possible to directly compare ERT changes and VWC measurements at specific locations. Finally, a 1-to-1 comparison of a 2-D HYDRUS hydrological model and changes in ERT during the irrigation event further confirmed the slight changes in ER at the TDR locations due to simultaneous wetting and root water uptake processes. However, the study highlights the critical role of the setting of the initial modelling conditions has on the final obtained results.

CRediT authorship contribution statement

Iael Raij Hoffman: Conceptualization, Data curation, Formal analysis, Investigation, Methodology, Project administration, Visualization, Writing – original draft, Writing – review & editing. **Daniela Vanella:** Conceptualization, Data curation, Investigation, Methodology, Supervision, Writing – original draft, Writing – review & editing. **Juan Miguel Ramirez Cuesta:** Data curation, Formal analysis, Methodology, Visualization, Writing – review & editing. **Srinivasa Rao Peddinti:** Data curation, Formal analysis, Investigation. **Isaya Kisekka:** Conceptualization, Funding acquisition, Methodology, Project administration, Resources, Writing – review & editing.

Declaration of competing interest

The authors declare that they have no known competing financial interests or personal relationships that could have appeared to influence the work reported in this paper.

Data availability

Data will be made available on request.

Acknowledgments

This study was supported by USDA NIFA Award # 2021-68012-35914, and by the projects "*E*-STRESS" (TED2021–131448A-I00), funded by MCIN/AEI/10.13039/501100011033 and the European Union NextGenerationEU/PRTR, and "DigitalRiego" (INNEST/2022/63) financed by the Agencia Valenciana de la Innovación (AVI) and the European Union (ERDF). We are grateful to the Button and Turkovich Farms for allowing us to conduct research on their farm.

Supplementary data

Supplementary data to this article can be found online at https://doi.org/10.1016/j.scitotenv.2023.169620.

References

Amato, M., Basso, B., Celano, G., Bitella, G., Morelli, G., Rossi, R., 2008. In situ detection of tree root distribution and biomass by multi-electrode resistivity imaging. Tree Physiol. 28 (10), 1441–1448.

Binley, A., Kemna, A., 2005. DC resistivity and induced polarization methods. In: Rubin, Y., Hubbard, S.S. (Eds.), Hydrogeophysics. Springer, Dordrecht.

Binley, A., Hubbard, S.S., Huisman, J.A., Revil, A., Robinson, D.A., Singha, K., Slater, L. D., 2015. The emergence of hydrogeophysics for improved understanding of subsurface processes over multiple scales. Water Resour. Res. 51 (6), 3837–3866.
Brillante, L., Mathieu, O., Bois, B., Van Leeuwen, C., Lévèque, J., 2015. The use of soil electrical resistivity to monitor plant and soil water relationships in vineyards. Soil 1 (1), 273–286.
California Department of Food, 2021. California Agricultural Production Statistics. Available at https://www.cdfa.ca.gov/Statistics/.
Campbell, G.S., Diak, G.R., 2005. Net and thermal radiation estimation and measurement. In: Micrometeorology in Agricultural Systems, 47, pp. 59–92.
Cassiani, G., Boaga, J., Vanella, D., Perri, M.T., Consoli, S., 2015. Monitoring and modelling of soil–plant interactions: the joint use of ERT, sap flow and eddy covariance data to characterize the volume of an orange tree root zone. Hydrol. Earth Syst. Sci. 19 (5), 2213–2225.
Chen, H., Niu, Q., 2022. Improving moisture content estimation from field resistivity measurements with subsurface structure information. J. Hydrol. 613, 128343.
Feddes, R.A., Kowalik, P.J., Zaradny, H., 1978. Simulation of Field Water Use and Crop Yield. John Wiley & Sons, New York, NY.
Garré, S., Javaux, M., Vanderborght, J., Pagès, L., Vereecken, H., 2011. Three-dimensional electrical resistivity tomography to monitor root zone water dynamics. Vadose Zone J. 10 (1), 412–424.
Geuzaine, C., Remacle, J.F., 2009. Gmsh: a three-dimensional finite element mesh generator with built-in pre- and post-processing facilities. Int. J. Numer. Methods Eng. 79 (11), 1309–1331.
Groenveld, T., Argaman, A., Šimůnek, J., Lazarovitch, N., 2021. Numerical modeling to optimize nitrogen fertigation with consideration of transient drought and nitrogen stress. Agric. Water Manag. 254, 106971.
Hanson, B., May, D., 2007. The effect of drip line placement on yield and quality of drip-irrigated processing tomatoes. Irrig. Drain. Syst. 21, 109–118. https://doi.org/10.1007/s10795-007-9023-5.
Hanson, B.R., Simůnek, J., Hopmans, J.W., 2006. Evaluation of urea-ammonium-nitrate fertigation with drip irrigation using numerical modeling. Agric Water Manag 86, 102–113. https://doi.org/10.1016/j.agwat.2006.06.013.
Heydari, L., Bayat, H., Castrignanò, A., 2023. Scale-dependent geostatistical modelling of crop-soil relationships in view of precision agriculture. Precis. Agric. https://doi.org/10.1007/s11119-023-09989-5.
Hilhorst, M.A., 2000. A pore water conductivity sensor. Soil Sci. Soc. Am. J. 64 (6), 1922–1925.
Idso, S.B., 1982. Non-water-stressed baselines: a key to measuring and interpreting plant water stress. Agric. Meteorol. 27 (1–2), 59–70.
Irmak, S., Haman, D.Z., Bastug, R., 2000. Determination of crop water stress index for irrigation timing and yield estimation of corn. Agron. J. 92 (6), 1221–1227.
Jackson, R.D., 1982. Canopy temperature and crop water stress. In: Advances in Irrigation, vol. 1. Elsevier, pp. 43–85.
Lazcano, C., Wade, J., Horwath, W.R., Burger, M., 2015. Soil sampling protocol reliably estimates preplant NO3- in SDI tomatoes. Calif. Agric. 69 (4), 222–229. https://doi.org/10.3733/ca.v069n04p222.
López-López, R., Arteaga-Ramírez, R., Vázquez-Peña, M.A., López-Cruz, I.L., Sánchez-Cohen, I., Ruiz-García, A., 2009. Crop water stress index for husk tomatoes (Physalis ixocarpa Brot.). Rev. Chapingo. Serie Horticult. 15 (3), 259–267.
López-López, R., Ramírez, R.A., Sánchez-Cohen, I., Bustamante, W.O., González-Lauck, V., 2011. Evapotranspiration and crop water stress index in Mexican husk tomatoes (Physalis ixocarpa Brot). In: Evapotranspiration—From Measurements to Agricultural and Environmental Applications, pp. 187–210.
Mary, B., Peruzzo, L., Iván, V., Facca, E., Manoli, G., Putti, M., Cassiani, G., 2021. Combining models of root-zone hydrology and geoelectrical measurements: recent advances and future prospects. Front. Water 3, 767910.
Michot, D., Benderitter, Y., Dorigny, A., Nicoullaud, B., King, D., Tabbagh, A., 2003. Spatial and temporal monitoring of soil water content with an irrigated corn crop cover using surface electrical resistivity tomography. Water Resour. Res. 39 (5).
Miller, E.E., Miller, R.D., 1956. Physical theory for capillary flow phenomena. J. Appl. Phys. 27 (4), 324–332.
Moreno, Z., Arnon-Zur, A., Furman, A., 2015. Hydro-geophysical monitoring of orchard root zone dynamics in semi-arid region. Irrig. Sci. 33, 303–318.
Mualem, Y., 1976. Hysteretical models for prediction of the hydraulic conductivity of unsaturated porous media. Water Resour. Res. 12, 1248–1254. https://doi.org/10.1029/WR012i006p01248.
Peddinti, S.R., Kisekka, I., 2022. Estimation of turbulent fluxes over almond orchards using high-resolution aerial imagery with one and two-source energy balance models. Agric Water Manag 269, 107671.
Raij-Hoffman, I., Miller, K., Paul, G., Yimam, Y., Mehan, S., Dickey, J., Harter, T., Kisekka, I., 2022. Modeling water and nitrogen dynamics from processing tomatoes under different management scenarios in the San Joaquin Valley of California. J. Hydrol. Region. Stud. 43 https://doi.org/10.1016/j.ejrh.2022.101195.
Rao, S., Lesparre, N., Flores-Orozco, A., Wagner, F., Kemna, A., Javaux, M., 2020. Imaging plant responses to water deficit using electrical resistivity tomography. Plant and Soil 454, 261–281.
Rimon, Y., Dahan, O., Nativ, R., Geyer, S., 2007. Water percolation through the deep vadose zone and groundwater recharge: preliminary results based on a new vadose zone monitoring system. Water Resour. Res. 43 (5) https://doi.org/10.1029/2006WR004855.
Rossi, R., Pollice, A., Bitella, G., Labella, R., Bochicchio, R., Amato, M., 2018. Modelling the non-linear relationship between soil resistivity and alfalfa NDVI: a basis for management zone delineation. J. Appl. Geophys. 159, 146–156.
Rouse, J.W., Haas, R.H., Schell, J.A., Deering, D.W., 1974. Monitoring vegetation systems in the Great Plains with ERTS. NASA Spec. Publ. 351 (1), 309.
Samouëlian, A., Cousin, I., Tabbagh, A., Bruand, A., Richard, G., 2005. Electrical resistivity survey in soil science: a review. Soil Tillage Res. 83 (2), 173–193.
Šimůnek, J., van Genuchten, M.T., Šejna, M., 2011. The HYDRUS Software Package for Simulating Two- and Three Dimensional Movement of Water, Heat and Multiple Solutes in Variably-Saturated Media, Technical Manual, Version 2.0.
Slater, L., Binley, A., Daily, W., Johnson, R., 2000. Cross-hole electrical imaging of a controlled saline tracer injection. J. Appl. Geophys. 44, 85–102.
Srayeddin, I., Doussan, C., 2009. Estimation of the spatial variability of root water uptake of maize and sorghum at the field scale by electrical resistivity tomography. Plant and Soil 319 (1–2), 185–207.
Tso, C.H.M., Kuras, O., Binley, A., 2019. On the field estimation of moisture content using electrical geophysics: the impact of petrophysical model uncertainty. Water Resour. Res. 55 (8), 7196–7211.
Tso, C.H.M., Johnson, T.C., Song, X., Chen, X., Kuras, O., Wilkinson, P., Binley, A., 2020. Integrated hydrogeophysical modelling and data assimilation for geoelectrical leak detection. J. Contam. Hydrol. 234, 103679.
Tsoulias, N., Gebbers, R., Zude-Sasse, M., 2020. Using data on soil ECa, soil water properties, and response of tree root system for spatial water balancing in an apple orchard. Precis. Agric. 21 (3), 522–548. https://doi.org/10.1007/s11119-019-09680-8.
van Genuchten, M.Th., 1980. A closed-form equation for predicting the hydraulic conductivity of unsaturated soils. Soil Sci. Soc. Am. J. https://doi.org/10.2136/sssaj1980.03615995004400050002x.
Vanella, D., Cassiani, G., Busato, L., Boaga, J., Barbagallo, S., Binley, A., Consoli, S., 2018. Use of small scale electrical resistivity tomography to identify soil-root interactions during deficit irrigation. J. Hydrol. 556, 310–324.
Vanella, D., Ramírez-Cuesta, J.M., Intrigliolo, D.S., Consoli, S., 2019. Combining electrical resistivity tomography and satellite images for improving evapotranspiration estimates of citrus orchards. Remote Sens. (Basel) 11 (4), 373.
Vanella, D., Ramírez-Cuesta, J.M., Sacco, A., Longo-Minnolo, G., Cirelli, G.L., Consoli, S., 2021. Electrical resistivity imaging for monitoring soil water motion patterns under different drip irrigation scenarios. Irrig. Sci. 39 (1), 145–157.
Vanella, D., Peddinti, S.R., Kisekka, I., 2022. Unravelling soil water dynamics in almond orchards characterized by soil-heterogeneity using electrical resistivity tomography. Agric Water Manag 269, 107652.
Vanella, D., Ramírez-Cuesta, J.M., Longo-Minnolo, G., Longo, D., D'Emilio, A., Consoli, S., 2023. Identifying soil-plant interactions in a mixed-age orange orchard using electrical resistivity imaging. Plant and Soil 1–17.
Vrugt, J.A., Van Wijk, M.T., Hopmans, J.W., Šimunek, J., 2001. One-, two-, and three-dimensional root water uptake functions for transient modeling. Water Resour. Res. 37, 2457–2470.
Waterhouse, H., Arora, B., Spycher, N.F., Nico, P.S., Ulrich, C., Dahlke, H.E., Horwath, W.R., 2021. Influence of Agricultural Managed Aquifer Recharge (AgMAR) and stratigraphic heterogeneities on nitrate reduction in the deep subsurface. Water Resour. Res. 57 (5) https://doi.org/10.1029/2020WR029148.